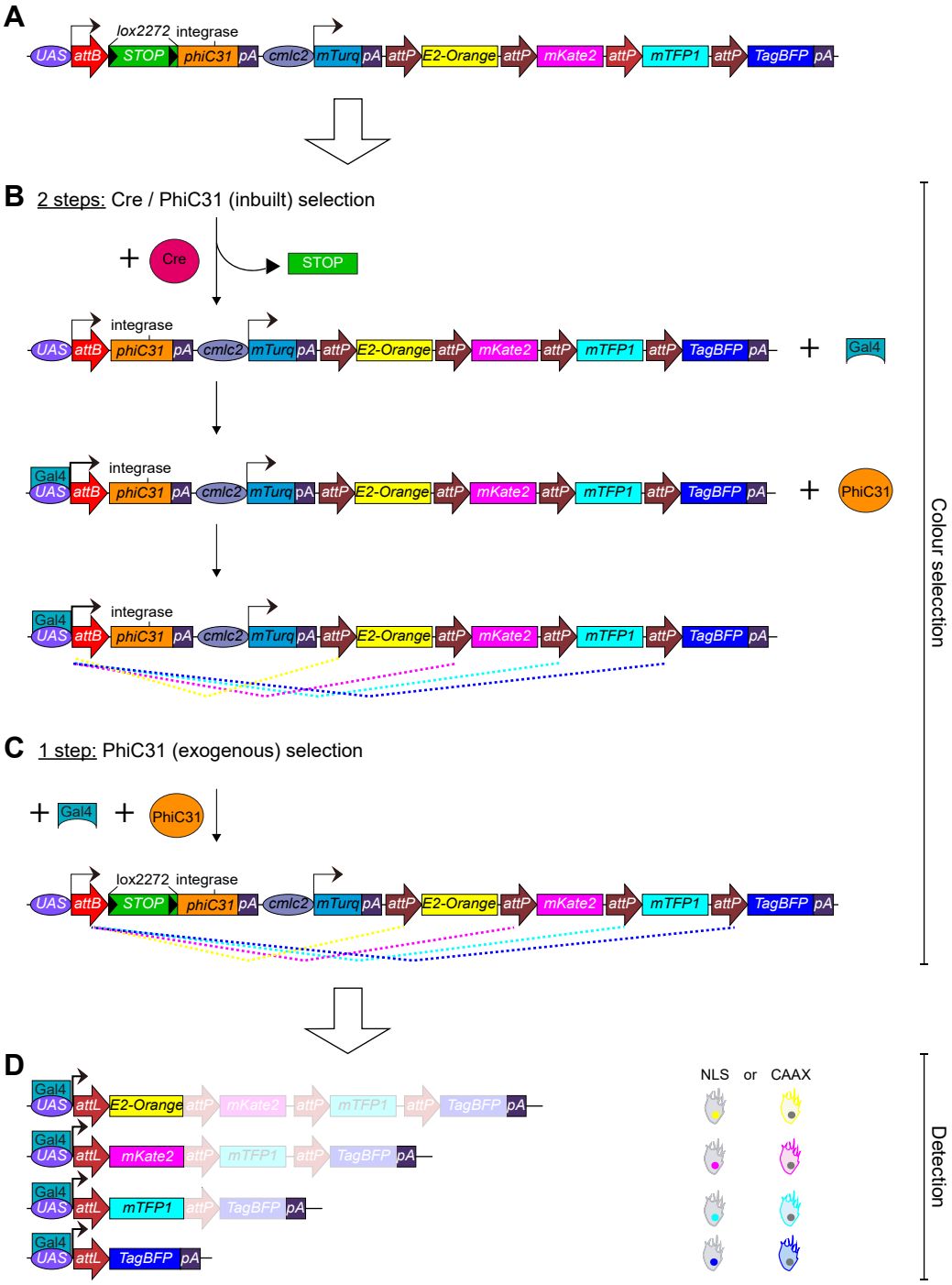

Fig. S1. Schematics of FRaeppli activation approaches. (A) Overview of the FRaeppli construct. Starting from the left: *5xUAS* can control expression of the selected FP, as well as the FRaeppli-inbuilt PhiC31 integrase. The following *attB* site can recombine with one of the four *attP* sites upstream of each FP. A STOP cassette flanked by two *lox2272* sites prevents uncontrolled expression of the *phiC31 integrase* gene, downstream of the *UAS*. Next, *cmlc2:mTurquoise* serves as genetic marker for the FRaeppli transgene and separates further the *attB* from *attP* sites, thereby ensuring a minimal bias of transgene selection. The *phiC31 integrase* gene is expressed after Cre-mediated excision of the STOP cassette. Lastly, the four FP genes, each equipped with an upstream *attP* site and a 3' STOP codon, are arranged

in a regular fashion and conclude with a single polyadenylation signal. (B) 2-step activation of FRaeppli colour selection: (i) Cre removal of the STOP cassette primes the FRaeppli cassette for recombination. Gal4 binding to the *5xUAS* activates the expression of *phiC31 integrase* gene, which (ii) can in turn recombine *attB* with one of the *attP* sites, self-excising the fragment in between, including the *phiC31 integrase* gene itself. (C) The addition of and exogenous source of PhiC31 integrase circumvents the need for Cre-medicated cassette excision and triggers *attB-attP* recombination in a one-step action. (D) Following colour selection, Gal4/UAS initiates the expression of the closest FP. Each FP gene ends with a stop codon, preventing expression of the remaining FPs, distal to the first one.

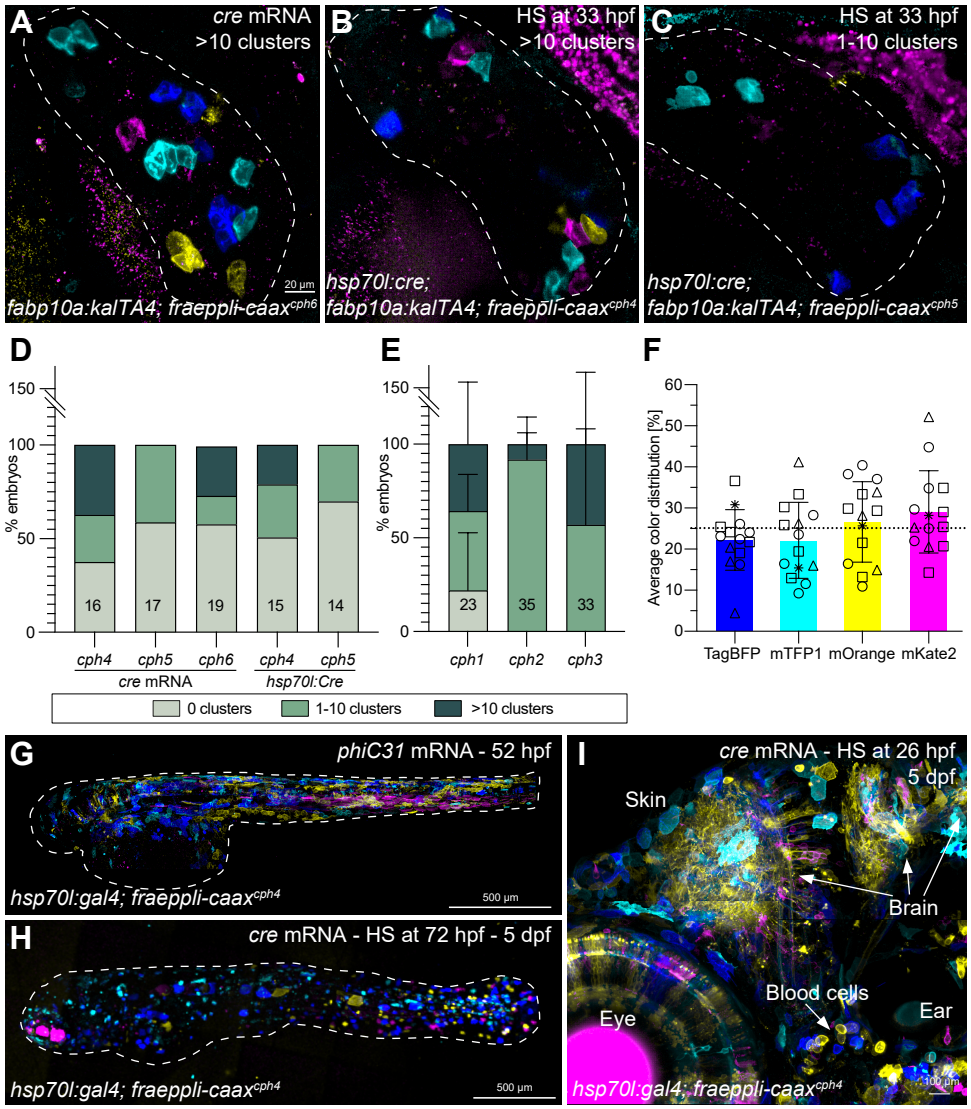

Fig. S2. Characteristics of *fraeppli-caax* and *fraeppli-nls* lines. (A-C) representative images of three independent *fraeppli-caax* lines activated by *cre* mRNA injection (A) or heat-shock-driven *cre* expression (B,C; N=1-3, n=2-13). (D) Quantification of cluster abundance in the three independent transgenic *fraeppli-caax* lines shown in A-C. *fraeppli-caax*^{cph4} exhibits the highest recombination efficiency, leading to the presence of >10 clusters per field of view in 37.5% of embryos. Transgenic lines *fraeppli-caax*^{cph6} and *fraeppli-caax*^{cph5} give rise to sparser labelling. Number of quantified embryos per condition is indicated in each column (N=1). (E) Quantification of cluster abundance in *fraeppli-nls; hsp70l:phiC31; fabp10a:kalTA4* embryos for three independent *fraeppli-nls* lines. Recombination was induced by heat-shock at 4 dpf, and analysis at 5 dpf shows slightly higher label density in *fraeppli-nls*^{cph1} and *fraeppli-nls*^{cph3}. Data are mean +s.d. (N=2, n≥23). (F) Quantification of colour selection frequency in *fraeppli-caax*^{cph4} livers Data are mean ±s.d (N=4; n=14). (G-H) Widespread FRAeppli expression in tissues throughout the embryo, following injections with *phiC31* (G; N=2, n=5) or heat-shock-induced recombination at 3 dpf (H; N=2, n=4). Note that at 52 hpf there is no apparent tissue bias, and all colours are expressed (related to Fig 2 H-I). (I) Close-up of the head region of a 5 dpf larvae, showing expression of FRaeppli in various tissues driven by a ubiquitous driver (related to Fig 2J; N=2, n=9).

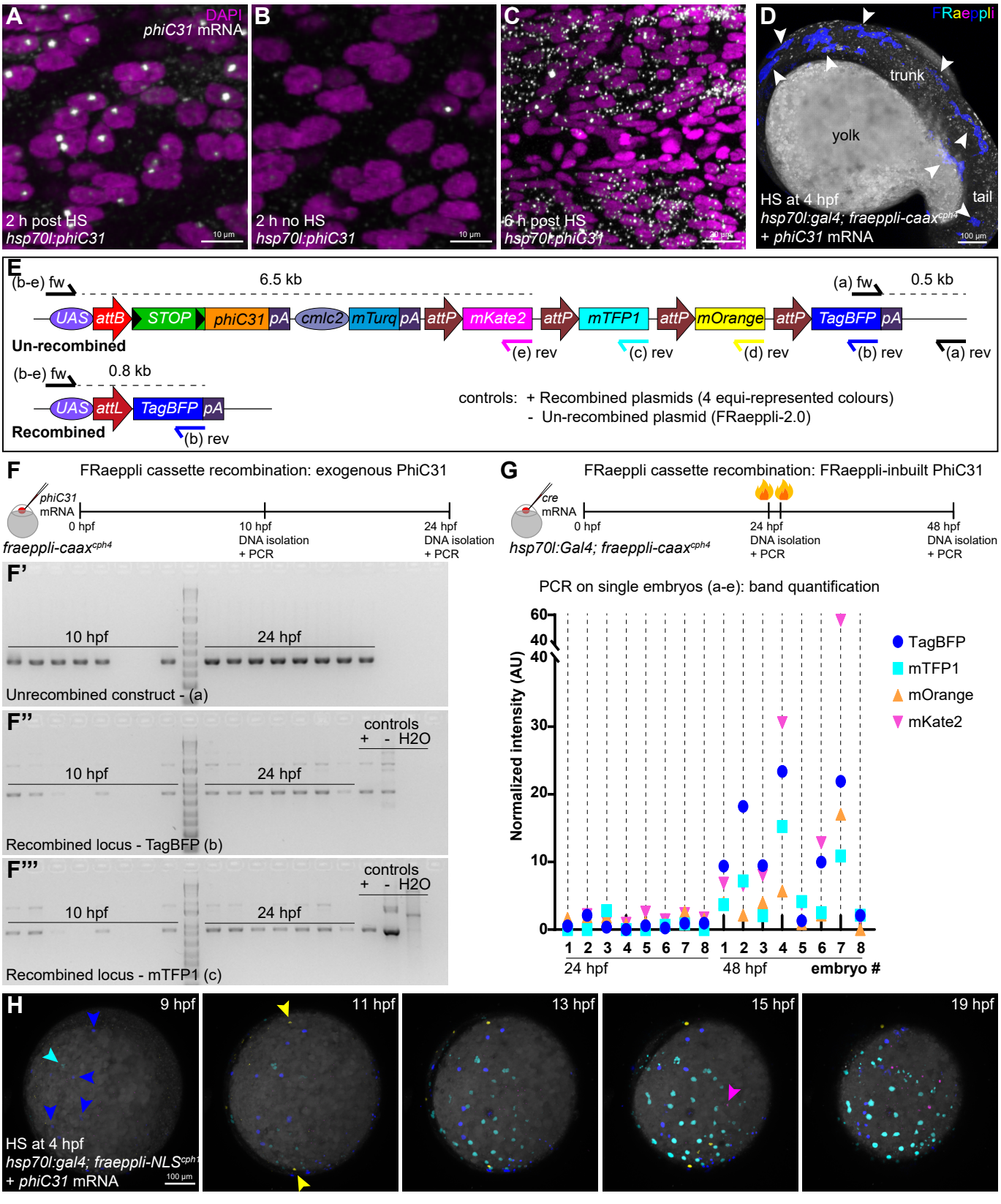

Fig. S3. PhiC31integrase recombines all four FRaeppli colours synchronously. (A-C) HCR staining showing *phiC31 integrase* mRNA expression in *hsp70l:phiC31* embryos 2 and 6 hours after heat-shock induction (A,C), compared to controls without heat-shock (B). Maximum intensity projections of confocal z-stacks of the trunk region. As expected, the HCR signal is nuclear at 2 hours and more cytoplasmic after 6 hours, since the mRNA molecules have already been exported from the nucleus (N=3, n=90). (D) TagBFP fluorescence can be detected prior to the other FPs in *fraeppli-caax;hsp70l:gal4* embryos injected with *phiC31 integrase* mRNA. *Live* imaging shows tagBFP signal already at 22 hpf (N=2, n=7). (E) Schematic representations of the genomic *fraeppli-caax* construct before and after PhiC31 Integrase-mediated recombination. (F) PCR on genomic DNA from 10 and 24 hpf *fraeppli-caax*^{cph4} single embryos activated by *phiC31 integrase* mRNA injection (n=16). (F') Primers 'a' amplify a common region of the FRaeppli construct, indicating the presence of the integrated transgene. Primer combinations 'b' and 'c' amplify only specific recombined forms of the FRaeppli transgene, when TagBFP (F'') or mTFP1 (F''') assume the first position after the promoter (schematic in E). Recombination for both colours is already detectable at 10 hpf detectable in all FRaeppli transgenic embryos. (G) PCR quantification of the recombined *fraeppli-caax* locus for all four colours, using the primer combinations indicated in (E). Recombination was triggered at 24 hpf by heat-shock-driven Gal4 expression, triggering inbuilt *phiC31 integrase* expression. 24 hours later (at 48 hpf), recombination for all colours was detected in 9/10 analysed embryos at variable degrees without bias, indicating synchronous and random colour-recombination (N=2, n=16). (H) Ventral view of an early embryo showing the timing of colour appearance in *fraeppli-nls*^{cph1}, following injections with *phiC31.* Two heat-shocks at 4 and 7 hpf were performed to maximize Gal4 expression. TagBFP- and mTFP1-positive cells are visible already at 9 hpf, when the timelapse started, followed by mOrange- (11 hpf) and mKate2-positive cells (15 hpf). Imaging and channel intensity parameters are maintained throughout the timepoints, displaying the incremental levels of each fluorescent protein in time. The relative timing of colour appearance varied slightly in different embryos, although the colour order remained the same (N=1, n=3). Colour abundance across embryos of a second similar experiment revealed that 60% of embryos display all four colours at 26 hpf (N=2; n=10) in *fraeppli-nls*^{cph1}. In the *fraeppli-caax*^{cph4} line colour appearance takes longer, with 27% and 9% of embryos showing 3 or 4 fluorescent proteins at 26 hpf, respectively, likely due to the dispersal of the fluorescent proteins in the membranes of the entire cell in addition to the high auto-fluorescence of the early embryonic tissues (N=2; n=11).

A

			Sequential Acquisition				Spectral Acquisition	
			Leica Stellaris 4 or 10 colors	Leica Stellaris 6 colors (live)	Zeiss LSM 880 6 colors (fixed)	Zeiss LSM 780 live timelapse	Zeiss LSM 780	Zeiss Multiphoton
FRaeppli FPs	EXCITATION	TagBFP	405 nm	405 nm	405 nm	405 nm	405 nm	1100 nm
		mTFP1	448 nm	448 nm	458 nm	458 nm	458 nm	1100 nm
		E2-Orange	547 nm	547 nm	514 nm	561 nm	561 nm	840 nm
		mKate2	589 nm	589 nm	594 nm	594 nm	561 nm	840 nm
	EMISSION	TagBFP	415 - 460nm	415 - 460 nm	410 - 464 nm	410 - 464 nm	Spectral Quasar detector*	Spectral Quasar detector*
		mTFP1	477 - 553 nm	477 - 487 nm	463 - 579 nm	464 - 499 nm	Spectral Quasar detector*	Spectral Quasar detector*
		E2-Orange	557 - 598 nm	557 - 598 nm	535 - 633 nm	570 - 597 nm	Spectral Quasar detector*	Spectral Quasar detector*
		mKate2	600 - 805 nm	600 - 622 nm	599 - 696 nm	597 - 695 nm	Spectral Quasar detector*	Spectral Quasar detector*
additional spectra	EX	green / GFP	-	488 nm	488 nm	-	-	-
		far-red	-	642 nm	633 nm	-	-	-
	EM	green / GFP	-	513 - 546 nm	520 - 575 nm	-	-	-
		far-red	-	660 - 790 nm	643 - 747 nm	-	-	-

* = 32 channels, 8.9 nm bandwidth, spectral range: 410nm - 694nm

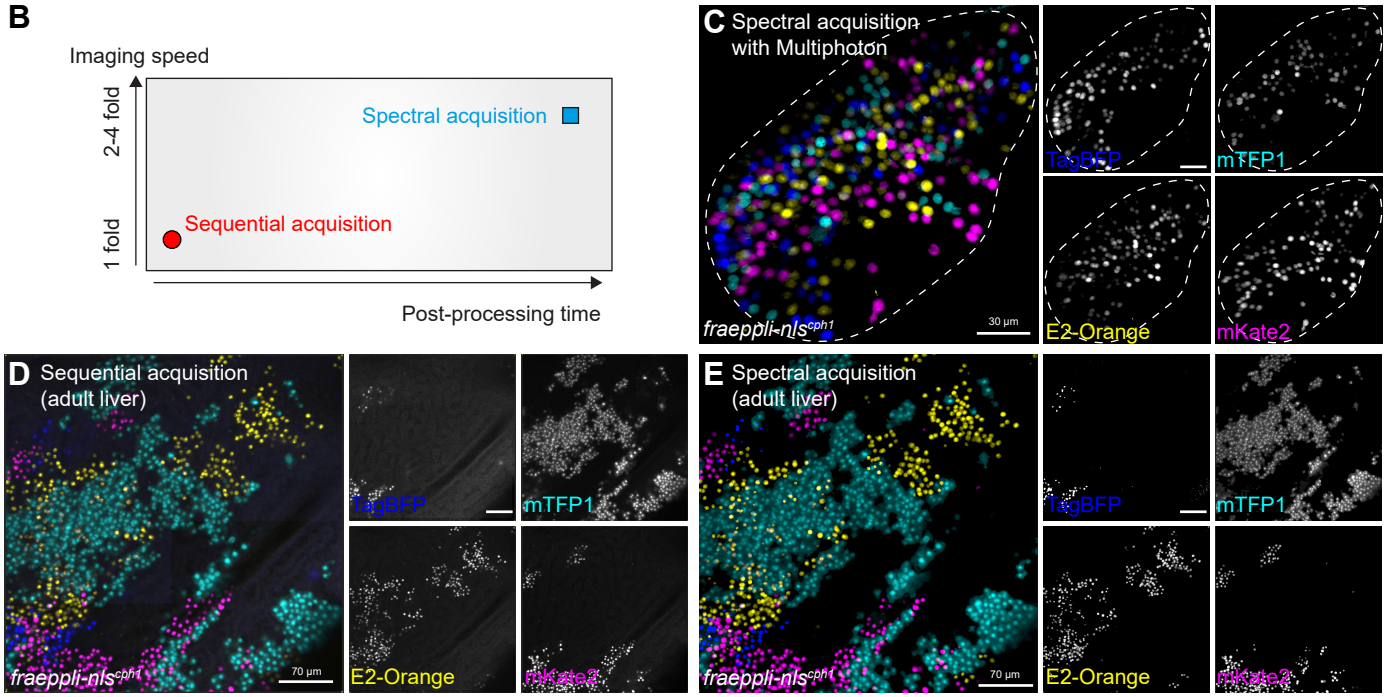

Fig. S4. Imaging configurations for spectral and sequential acquisition. (A) Sequential and spectral FRaeppli acquisition settings for the microscope set-ups used in this study. (B) Schematic showing the inverse behaviour of imaging speed and post-processing time when applying spectral and sequential imaging modes. (C) Spectral acquisition with 2-photon excitation using two wavelengths is sufficient to excite all four FPs expressed in the liver at 4 dpf from *fraeppli-nls;prox1a:kalTA4* injected with *cre* mRNA (N=3, n=10). (D) Sequential and (E) spectral acquisition followed by unmixing using hyperspectral phasor analysis show comparable detection outcomes for all FPs in liver sections from adult *fraeppli-nls;prox1a:kalTA4* zebrafish. Embryonic *cre* mRNA injection triggered FRaeppli recombination (n=3).

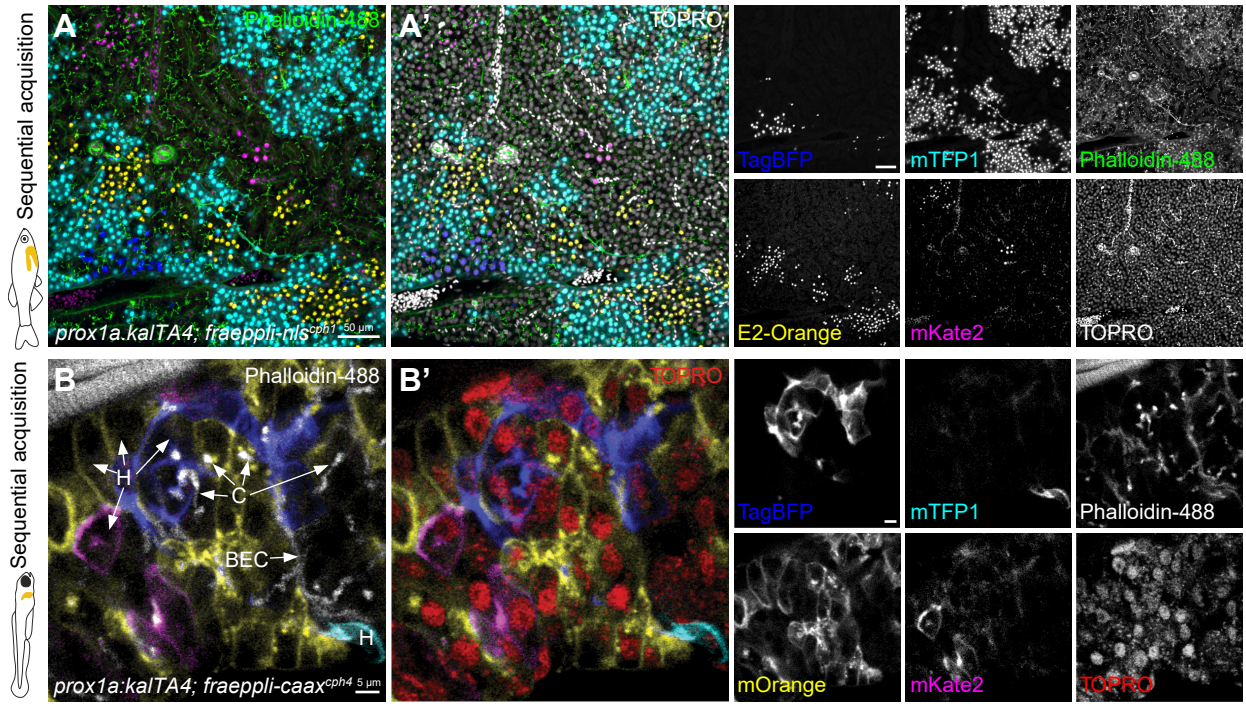

Fig. S5. Advanced labelling approaches for FRaeppli with spectrally-distinct markers for visualizing tissue context. (A,B) Maximum intensity projections of sequentially acquired liver tissue from *fraeppli-nls;prox1a:kalTA4* adults cleared using the SeeDB2 protocol (A; N=1), and *fraeppli-caax;prox1a:kalTA4* 5 dpf larvae (B). Beyond FRaeppli, tissue was stained for Actin (Phalloidin-488, green) and the nucleus (TO-PRO, red) to visualize tissue architecture at the cellular and subcellular level. Embryonic *cre* mRNA injection triggered FRaeppli recombination (N=2, n=8).

Table S1

Primer #	Sequence
86	TAATACGACTCACTATAGG
170	CTGCAGGTCGGAGTACTGTC
267	AATTGAATTGCGCTGATGC
327	CACTTTGTGTTGAGCGG
331	TTGGTCGGTCATTTCGG
332	CTATCGGCCGCCTAGGTAGGGATAACAGGGTAATACCGGTC CTGCAGGTCGGAGTACTGT
333	ATCGAATTCGTGTGGAGGAG
334	CTAGTCTAGAAGTGAGTCGTATTACGTAGATCC
335	CTAGACTAGTTAGGGATAACAGGGTAATCGAATTAAAAAACCT CCCAC
336	TTAAGGAAGTAAAAGTAAAAGCAAGAA
340	TGTACAGGTTCTTTCCGCCTCAGAA
341	ACCTCCAGGTTGATGGTGTT
342	CCTGAAGGGCAAGATCAAGA
343	ACGGCACCTTCATCTACCAC
346	GTTCAGGATCTCGATGCGGTG
347	AAGAACATCGATTTTCCATGGCAG
348	TTTATACGAAGTTATCCTAGCATGCA
349	GTATCCTATACGAAGTTATTTACATATGC
350	GCGTGCCTGATCTTGTTGAA
351	CTATATGCATCAAGCAAACATGGACACGTACGCGGGTG
353	CTAGGCTAGCGCAGGCCTAAATCAGTTGTG
355	CCGGGATCACTCTCGGCAT
356	GACCAACAGCAAAGCAGACA
371	ATATGGCGCGCCTATGGTGAGCAAGGGCGAG
372	CTAGCTACATATGCTTGTACAGCTCGTCCATGCC
382	GAAATGCCCGACGAACCTG
581	CACATGAAGCAGCACGACTTCT
613	CTAATATCGATTTCTGCAGCCCGGGGGATC
614	ATACATGCATGCTCTAGAGGCTCGACTGC
615	CGCTGAGTGGTATGAGCTTC
617	CTAGGGTACCTCAACCACTCCAGGCATAGC
618	TATACCGCGGGATCTGGCCATCTAGAGCGG
623	TTATGGATCCCAAGCAAACATGGACACGTACG
624	ATATGGGCCCACTTGGTTCCAGCGCCGCTACGTCTTCCGTG
628	TTATGGGCCCATGGTGAGCAAGGGCGAGG
629	ATATGGGCCCTCAACGGGGAACCCGAAGC
650	ATATGGATCCGGGCCCATGGTGAGCAAGGGCGAG
651	ATATCTGCAGACGGGGAACCCGAAGCTC
662	TATATGTGGTCTTGATGTTTGC
663	ACTGCTCCACCACGGTG
664	GCTTCAGCCTCATCTTGATCTT
666	GGAGCCATCTGATCGCAA
667	TAGGGATAACAGGGTAATCGAATT

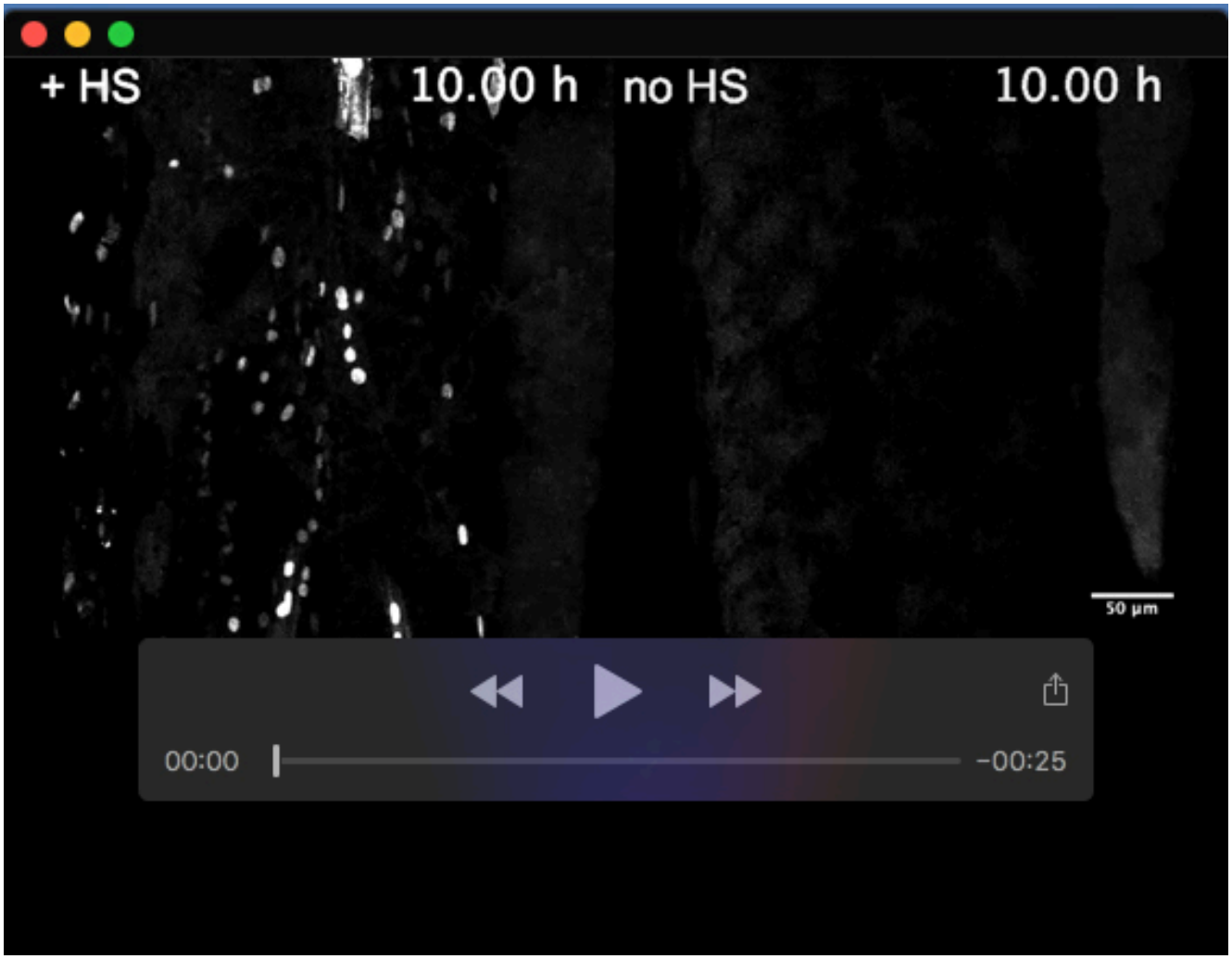

Movie 1. Maturation dynamics of phiC31-sfGFP-NLS. Time-series of *hsp70l:phiC31-sfGFP-nls*, which can be detected from around 2 hours after heat-shock and the expression peaks at 6 hours. Without heat-shock transgene expression is undetectable (N=2, n=4).

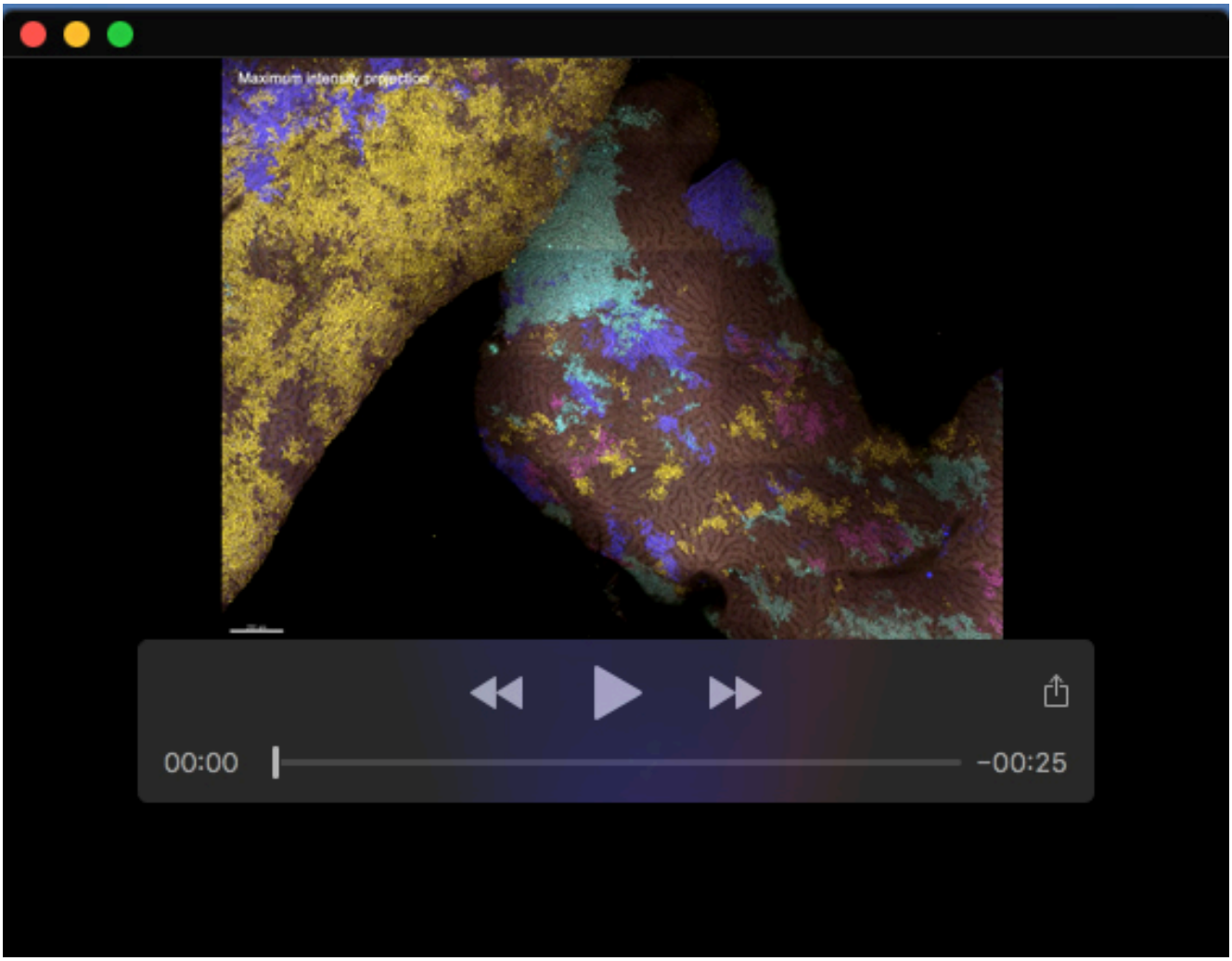

Movie 2. FRaeppli-NLS labelling of adult tissues. Endogenous FRaeppli-NLS fluorescence is well preserved with SeeDB2 clearing and detectable beyond 120 μm, while the fluorescent signal disappears after only 30 μm of depth without clearing (n=2).

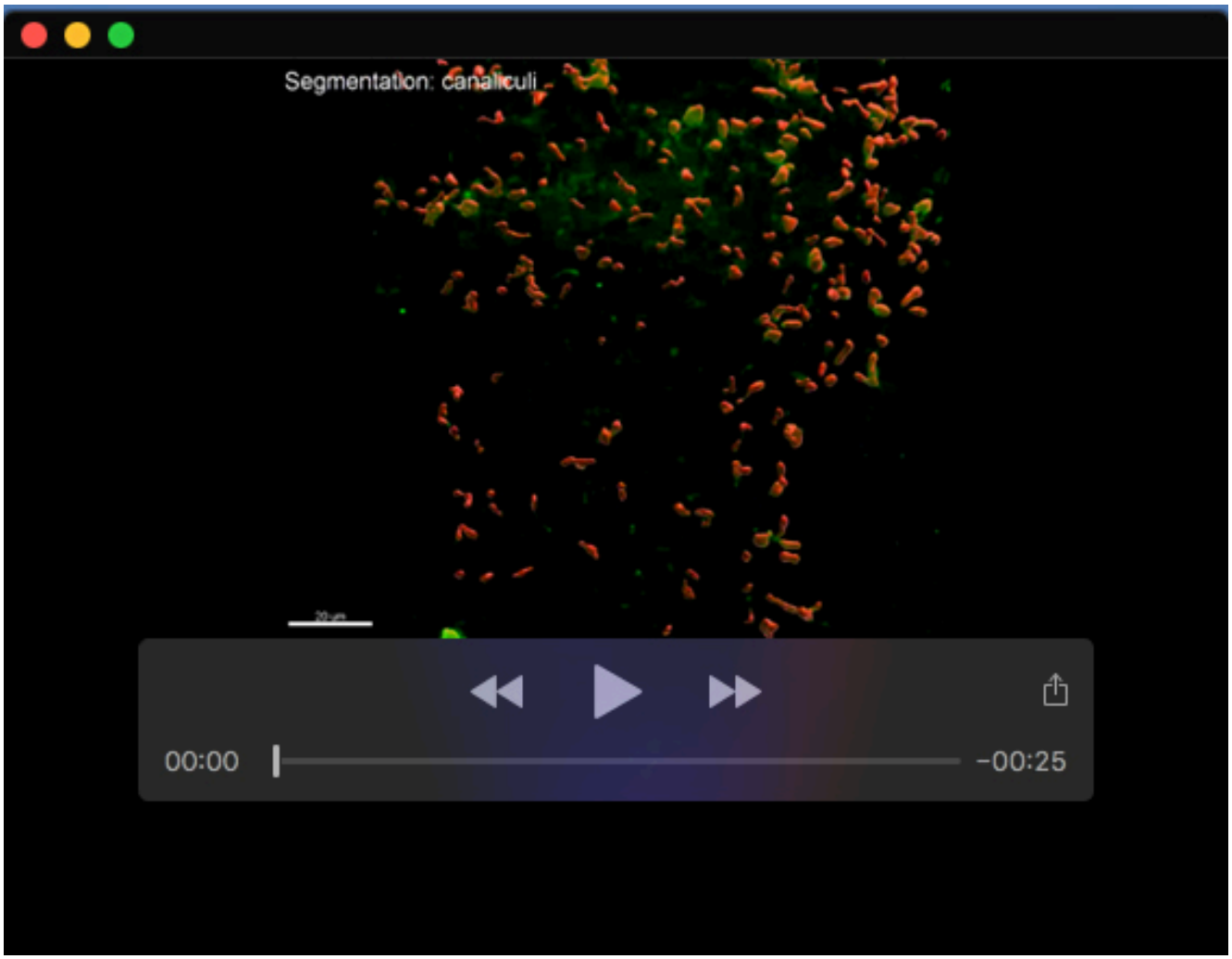

Movie 3. Stepwise analysis of canalicular topologies in 5 dpf zebrafish livers. FRaeppli-CAAX combined with α-Mdr1 staining (Alexa 488) undergoes sequential segmentation and topological analysis of hepatocyte canaliculi in larvae (see also Supplementary Methods), including examples of distinct canalicular topologies.

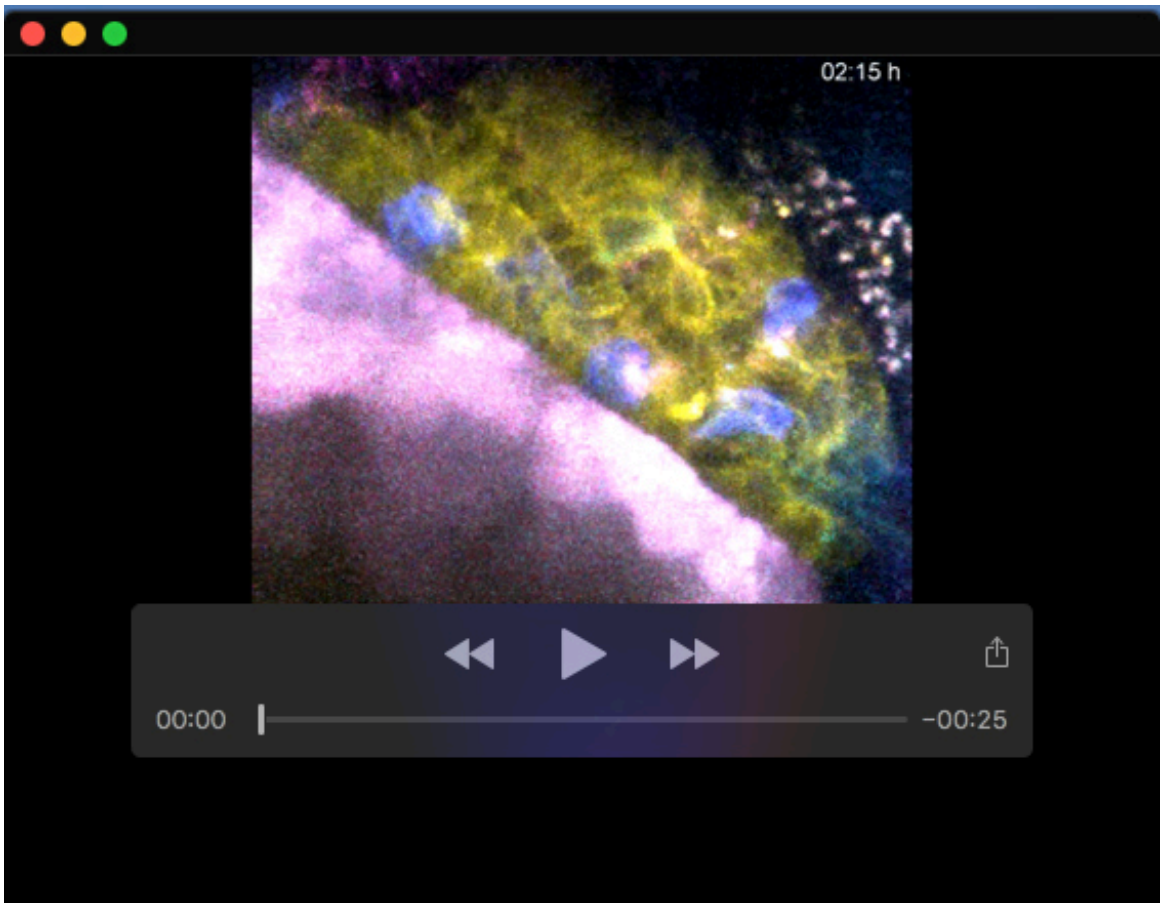

Movie 4. Time-lapse of dynamic liver cell rearrangement in a 72 hpf *fraeppli-caax* embryo. A Tag-BFP cell (arrow at the beginning of the movie) loses contact with its clonal neighbour and moves 2-3 cell diameter away. Simultaneous labelling of cells in different colours allows studying cell movements in the cellular context (N=3, n=10).

References:

Bischof, J., Maeda, R. K., Hediger, M., Karch, F. and Basler, K. (2007). An optimized transgenesis system for Drosophila using germ-line-specific phiC31 integrases. *Proc Natl Acad Sci U S A* **104**, 3312-3317.

Cayuso, J., Dzementsei, A., Fischer, J. C., Karemore, G., Caviglia, S., Bartholdson, J., Wright, G. J. and Ober, E. A. (2016). EphrinB1/EphB3b Coordinate Bidirectional Epithelial-Mesenchymal Interactions Controlling Liver Morphogenesis and Laterality. *Dev Cell* **39**, 316-328.

Choi, H. M., Calvert, C. R., Husain, N., Huss, D., Barsi, J. C., Deverman, B. E., Hunter, R. C., Kato, M., Lee, S. M., Abelin, A. C., et al. (2016). Mapping a multiplexed zoo of mRNA expression. *Development* **143**, 3632-3637.

Choi, H. M. T., Schwarzkopf, M., Fornace, M. E., Acharya, A., Artavanis, G., Stegmaier, J., Cunha, A. and Pierce, N. A. (2018). Third-generation in situ hybridization chain reaction: multiplexed, quantitative, sensitive, versatile, robust. *Development* **145**.

Cutrale, F., Trivedi, V., Trinh, L. A., Chiu, C. L., Choi, J. M., Artiga, M. S. and Fraser, S. E. (2017). Hyperspectral phasor analysis enables multiplexed 5D in vivo imaging. *Nat Methods* **14**, 149-152.

Distel, M., Wullimann, M. F. and Koster, R. W. (2009). Optimized Gal4 genetics for permanent gene expression mapping in zebrafish. *Proc Natl Acad Sci U S A* **106**, 13365-13370.

Felker, A. and Mosimann, C. (2016). Contemporary zebrafish transgenesis with Tol2 and application for Cre/lox recombination experiments. *Methods Cell Biol* **135**, 219-244.

Feng, H., Langenau, D. M., Madge, J. A., Quinkertz, A., Gutierrez, A., Neuberg, D. S., Kanki, J. P. and Look, A. T. (2007). Heat-shock induction of T-cell lymphoma/leukaemia in conditional Cre/lox-regulated transgenic zebrafish. *Br J Haematol* **138**, 169-175.

Her, G. M., Yeh, Y. H. and Wu, J. L. (2003). 435-bp liver regulatory sequence in the liver fatty acid binding protein (L-FABP) gene is sufficient to modulate liver regional expression in transgenic zebrafish. *Dev Dyn* **227**, 347-356.

Jin, S. W., Beis, D., Mitchell, T., Chen, J. N. and Stainier, D. Y. (2005). Cellular and molecular analyses of vascular tube and lumen formation in zebrafish. *Development* **132**, 5199-5209.

Kanca, O., Caussinus, E., Denes, A. S., Percival-Smith, A. and Affolter, M. (2014). Raeppli: a whole-tissue labeling tool for live imaging of Drosophila development. *Development* **141**, 472-480.

Kawakami, K., Shima, A. and Kawakami, N. (2000). Identification of a functional transposase of the Tol2 element, an Ac-like element from the Japanese medaka fish, and its transposition in the zebrafish germ lineage. *Proc Natl Acad Sci U S A* **97**, 11403-11408.

Ke, M. T., Nakai, Y., Fujimoto, S., Takayama, R., Yoshida, S., Kitajima, T. S., Sato, M. and Imai, T. (2016). Super-Resolution Mapping of Neuronal Circuitry With an Index-Optimized Clearing Agent. *Cell Rep* **14**, 2718-2732.

Koltowska, K., Lagendijk, A. K., Pichol-Thievend, C., Fischer, J. C., Francois, M., Ober, E. A., Yap, A. S. and Hogan, B. M. (2015). Vegfc Regulates Bipotential Precursor Division and Prox1 Expression to Promote Lymphatic Identity in Zebrafish. *Cell Rep* **13**, 1828-1841.

Mosimann, C., Puller, A. C., Lawson, K. L., Tschopp, P., Amsterdam, A. and Zon, L. I. (2013). Site-directed zebrafish transgenesis into single landing sites with the phiC31 integrase system. *Dev Dyn* **242**, 949-963.

Ni, T. T., Lu, J., Zhu, M., Maddison, L. A., Boyd, K. L., Huskey, L., Ju, B., Hesselson, D., Zhong, T. P., Page-McCaw, P. S., et al. (2012). Conditional control of gene function by an invertible gene trap in zebrafish. *Proc Natl Acad Sci U S A* **109**, 15389-15394.

Parsons, M. J., Pisharath, H., Yusuff, S., Moore, J. C., Siekmann, A. F., Lawson, N. and Leach, S. D. (2009). Notch-responsive cells initiate the secondary transition in larval zebrafish pancreas. *Mech Dev* **126**, 898-912.

Poulain, M. and Ober, E. A. (2011). Interplay between Wnt2 and Wnt2bb controls multiple steps of early foregut-derived organ development. *Development* **138**, 3557-3568.

Reddy, V. B., Ghosh, P. K., Lebowitz, P., Piatak, M. and Weissman, S. M. (1979). Simian virus 40 early mRNA's. I. Genomic localization of 3' and 5' termini and two major splices in mRNA from transformed and lytically infected cells. *J Virol* **30**, 279-296.

Rupp, R. A., Snider, L. and Weintraub, H. (1994). Xenopus embryos regulate the nuclear localization of XMyoD. *Genes Dev* **8**, 1311-1323.

Soroldoni, D., Hogan, B. M. and Oates, A. C. (2009). Simple and efficient transgenesis with meganuclease constructs in zebrafish. *Methods Mol Biol* **546**, 117-130.

Team, R. (2019). RStudio: Integrated Development for R.: RStudio, Inc., Boston, MA

Team, R. C. (2020). R: A language and environment for statistical computing.: R Foundation for Statistical Computing, Vienna, Austria.

Thestrup, M. I., Caviglia, S., Cayuso, J., Heyne, R. L. S., Ahmad, R., Hofmeister, W., Satriano, L., Wilkinson, D. G., Andersen, J. B. and Ober, E. A. (2019). A morphogenetic EphB/EphrinB code controls hepatopancreatic duct formation. *Nat Commun* **10**, 5220.

Urasaki, A., Morvan, G. and Kawakami, K. (2006). Functional dissection of the Tol2 transposable element identified the minimal cis-sequence and a highly repetitive sequence in the subterminal region essential for transposition. *Genetics* **174**, 639-649.

Westerfield, M. (2000). *The Zebrafish Book: A Guide for the Laboratory Use of Zebrafish (Danio rerio).* : University of Oregon Press, Eugene, OR.